Title

A 3D individual-based model to investigate the spatially heterogeneous response of bacterial biofilms to antimicrobial agents

Lakshmi Machineni, Ch. Tejesh Reddy, Vandana Nandamuri, Parag D. Pawar
Department of Chemical Engineering, Indian Institute of Technology Hyderabad, India

Corresponding Author
Parag D. Pawar
Department of Chemical Engineering
Indian Institute of Technology Hyderabad
Kandi, Sangareddy – 502285
Telangana 502 205, India
Tel.: +91 40 2301 6068
Fax: +91 40 2301 6032
Email: parag@iith.ac.in

Keywords: biofilms; antibiotic resistance; cellular automata; heterogeneity;

Abstract

The response of bacterial biofilms to treatment with antimicrobial agents is often characterized by the emergence of recalcitrant cellular microcolonies. We present an individual-based model to investigate the biophysical mechanisms of the selective resistance that arises within the biofilm and leads to a spatially heterogeneous response upon treatment with antibiotics. The response occurs in three distinct phases. In the first phase, the subpopulation of metabolically active cells diminishes due to antibiotic-induced cell death. Subsequently, in the second phase, increased nutrient availability allows dormant cells in the lower layers of the biofilm to transform into metabolically active cells. In the third phase, survival of the biofilm is governed by the interplay between two contrasting factors: (i) rate of antibiotic-induced cell death, and (ii) rate of transformation of dormant cells into active ones. Metabolically active cells at the distal edge of the biofilm sacrifice themselves to protect the dormant cells in the interior by (i) reducing local antibiotic concentrations, and (ii) increasing nutrient availability. In the presence of quorum sensing, biofilms exhibit increased tolerance compared to the quorum sensing-negative strains. EPS forms a protective layer at the top of the biofilm, thereby limiting antibiotic penetration. The surviving cells, in turn, produce EPS resulting in a feedback-like mechanism of resistance. Whereas resistance in QS^- biofilms occurs because of transformation of dormant cells into metabolically active cells, this transformation is less pronounced in QS^+ biofilms, and resistance is a consequence of the sequestration of the antibiotic by EPS.

Introduction

Biofilms are surface-associated communities of microorganisms embedded in an extracellular matrix composed primarily of self-produced polysaccharides [1, 2]. Biofilms shelter bacteria from environmental stresses and from the host immune response, thereby increasing resistance to antibiotics and phagocytosis, as well as to other components of the innate and adaptive immune systems [3, 4]. Several mechanisms -- acting synergistically -- contribute to the reduced antimicrobial and biocide susceptibility that is characteristic of biofilm communities. Expression of specific genes may allow biofilm bacteria to actively adapt to, and survive, antimicrobial exposure [5-9]. For instance, the *ndvB* locus has been identified as a *Pseudomonas aeruginosa* (*P. aeruginosa*) biofilm-specific antibiotic resistant gene; *ΔndvB* biofilms were 16-fold more susceptible to tobramycin and 8-fold more susceptible to both gentamicin and ciprofloxacin than wild-type biofilms [10]. In response to antibiotic treatment, overexpression of toxins that inhibit essential functions such as translation may contribute to the transformation of biofilm bacteria to an antibiotic tolerant phenotype [11]. These genetic mechanisms attribute resistance of the biofilm to antibiotic tolerance at the single-cell level [12, 13].

Antibiotic resistance may also emerge as a consequence of physiological characteristics inherent to the biofilm mode of growth [1, 14]. Biofilms are characterized, among other things, by the presence of nutrient and antibiotic gradients, diffusion and penetration limitations, and a matrix of extracellular polymeric substances (EPS) [15-17]. Bacteria growing in biofilms are physiologically heterogeneous, due in part to their adaptation to local environmental conditions. They occupy a spectrum of growth states from rapidly growing and active to slow-growing and dormant. Consequently, distinct microcolonies with clusters of bacterial cells may develop within the biofilm where cellular physiology is different from surroundings in terms of metabolic activity, secretion of EPS, and concentrations of nutrients and antimicrobial agents [17-20]. This intrinsic physiological heterogeneity of biofilms may play a role in the adaptive stress response, and contribute to the protection of cells [21]. Experimental evidence suggests that it is only certain subpopulations within biofilms that show greatly increased phenotypic resistance to treatment, whereas the remaining cells exhibit sensitivity [22-24]. A particular antimicrobial agent may effectively target certain populations of cells, but leave the remaining cells viable, allowing them to repopulate the biofilms when the treatment is stopped. For instance, cells deep within *P. aeruginosa* biofilms are reported to be in a metabolically inactive, antibiotic-tolerant state, whereas cells at the periphery are faster growing, and susceptible to antimicrobial agents such as ciprofloxacin, tetracycline, and tobramycin [25, 26]. The biophysical mechanisms underlying this spatially non-uniform response of biofilms to antimicrobial treatment remain incompletely understood.

The lowest concentration of the antimicrobial agent required to eradicate the biofilm is termed the minimum biofilm eradication concentration (MBEC) [27]. Subjecting the biofilm to sub-lethal concentrations of the antibiotic (sub-MBEC) enhances biofilm formation *in vitro* [28-30]. For instance, subjecting *P. aeruginosa* biofilms to sub-MBEC treatment induces genetic triggers that result in the enhanced formation of colonic acid [31]. This, in turn, causes an increase in the synthesis of EPS which contributes to the protection of the bacterial population. Antibiotic-induced biofilm formation has clinical relevance because bacteria are exposed to low concentrations of antibiotics at the beginning and the end of treatment, or continuously during low-dose therapy [30]. Investigating the reasons for survival of biofilms in response to sub-

MBEC treatment of antibiotics may help delineate biophysical mechanisms of antibiotic resistance.

Quorum sensing (QS) is a process by which bacteria coordinate their behavior in a cell-density dependent manner by producing and detecting signaling molecules called autoinducers [32-34]. QS has been shown to control the amount of EPS synthesis in *P. aeruginosa* biofilms [35-39]. Furthermore, experimental investigations support the role of QS-regulated EPS in the resistance of *P. aeruginosa* biofilms to antibiotic treatment [40]. The EPS matrix protects the biofilm by impeding penetration of tobramycin via ionic interactions at the periphery [39, 41]. In addition, antibiotic susceptibility of *Staphylococcus aureus* biofilms towards vancomycin increases in the presence of QS-inhibitors by deactivating EPS biosynthesis [42]. Nutrient concentration gradients in QS^+ biofilms may induce spatio-temporal heterogeneity in autoinducer secretion, which may, in turn, result in microscale variation in EPS production. How the spatial heterogeneity of EPS influences the heterogeneous response of biofilms to antibiotics is currently not known.

We have previously formulated and analyzed a three-dimensional, individual-based computational model to simulate biofilm growth dynamics, and to quantify spatial heterogeneity in the bacterial population as a function of nutrient availability and quorum sensing [43]. The model treats bacterial cells as individual entities with their own states, thereby allowing for variability between individual behaviors with respect to their growth rates, antibiotic and nutrient uptake rates, autoinducer production, up-regulation and down-regulation states, and EPS secretion. The individual-based, discrete nature of the model, combined with physical dynamics causes chemical and structural heterogeneities within the biofilm to emerge as a consequence of the actions and interactions of the cells with each other, and with the surrounding environment, rather than being a model input. In this work, we investigate the response of QS^- and QS^+ biofilms to treatment with antibiotics, and the influence of heterogeneity on this response. The goal was to answer the following questions: (1) Do local physiological and chemical heterogeneities in the biofilm influence the spatially heterogeneous antibiotic resistance in the absence of genetic triggers? (2) What roles do biophysical and cellular processes play in enhanced biofilm formation in response to treatment with sub-lethal doses of antibiotics? (3) What role does EPS play in the heterogeneous response of the biofilm to antibiotic treatment? Our results indicate that during the initial stages of treatment, the proportion of the fast-growing, metabolically active subpopulation decreases due to exposure to the antibiotic. This results in an increase in the nutrient availability to the dormant cells in the inner regions of the biofilm. We propose that this triggers a transformation from the dormant state to the metabolically active state, and that this transformation is a key mechanism of resistance. When subjected to sub-MBEC treatment, antibiotic-induced cell death at the biofilm surface leads to increased nutrient availability in the inner regions, resulting in enhanced growth compared to the untreated biofilm. Due to the protective influence of EPS, QS^+ biofilms required a higher concentration of the antibiotic to eradicate compared to the QS^- biofilms.

Methods

Model description and simulation domain

We used a 3D individual-based model to simulate the growth dynamics of a bacterial biofilm in response to treatment with antibiotics. Biofilm growth is simulated within a rectangular box whose bottom surface (120 μm x 120 μm) represents the inert substratum. A reservoir of nutrient is placed at the top at a constant distance from the substratum, and is continuously replenished so that a constant concentration is maintained in the bulk phase. The interface between the reservoir and the biofilm domain is termed the diffusion boundary layer (DBL). The space between the DBL and the substratum is discretized into cubical elements of volume 27 μm^3 each. During the simulation, each element may be occupied by one or more of the following entities: (i) bacterial cell, (ii) EPS, (iii) nutrient, (iv) autoinducer, and (v) antibiotic. Periodic boundary conditions are applied in the horizontal directions, thereby eliminating edge effects, and ensuring continuity of biomass [44, 45]. Each bacterium is modeled as a distinct entity with its own set of parameter values and behaviors. To simulate behavioral variability, parameter values for individual bacterial cells are obtained by random draws from a uniform distribution around the values listed in Table 1. The simulation represents a time march in which the occupancy state of each element is updated at every time step. At time t = 0, six cells, termed colonizers, are placed into random elements atop the substratum. Simultaneously, nutrient diffuses across the DBL. Cells consume nutrient, and subsequently grow and divide, resulting in the formation of a contiguous multicellular population. At the end of each time step, the nutrient reservoir is shifted vertically upwards such that a pre-determined distance from the topmost cell in the biofilm is always maintained.

Assumptions

The following are the key assumptions made:

(1) The biofilm does not pose an obstacle to flow, and is subjected to a constant linear velocity gradient of 10 s^{-1} with zero velocity at the substratum, and maximum velocity at the highest point. It has been shown that giving up the conservation principles for fluid flow in the biofilm domain leads to increased deviations with respect to concentration fields and fluxes [46]. The magnitude of deviation is in some cases small (< 2%, at slow bulk flow velocities of ~0.0001 ms^{-1}), and considerable in other (> 20%, at fast bulk flow velocities of 0.01 ms^{-1}). The results presented in this work correspond to the low bulk flow regime (maximum velocity of ~0.0006 ms^{-1}). Consequently, deviations in concentration fields and fluxes have been neglected. Such low fluid shear rates (10-50 s^{-1}), experienced within the intestine, and veins, have been shown to be effective in simulating S. aureus biofilm colonization and development [47, 48].

(2) The DBL remains parallel to the substratum throughout the simulation. It is worth noting that at high fluid velocities, the diffusion boundary could follow the surface of the biofilm, and may not be necessarily stratified as is assumed here [49].

(3) The DBL has a constant thickness of 18 μm. For the low-flow regime considered in this work, the nutrient concentration at a vertical distance of 18 μm from the highest cell in the

biofilm was greater than 95% of the bulk nutrient concentration, even at time points corresponding to the highest cell numbers.

(4) EPS is capable of coexisting with a bacterial cell within a cubical element. This is consistent with previous experimental work showing the accumulation of extracellular polysaccharides such as β-glucan found intercalating between micro colonies of *Streptococcus mutans* [50]. Consequently, we assume that new bacterial cells embed themselves into existing EPS, instead of pushing it aside.

(5) Negative parameter values of individual bacterial cells, or those outside ±10% of the mean were discarded; these precautions are necessary with distributions ranging from $-\infty$ to $+\infty$.

A full mathematical description of the various components and processes incorporated in the model has been presented elsewhere [43]. Here, we briefly present the governing equations, behaviors of the particulate and soluble entities, and the numerical scheme used.

Nutrient reaction and transport

The rate of consumption of the nutrient by bacteria is a function of the concentrations of the biomass ($C_B(\bar{x},t)$) and the nutrient $C_N(\bar{x},t)$ at the spatial coordinates $\bar{x}$ and time t, and is given by

$$r_N(\bar{x},t) = \left(\frac{\mu_{max}}{Y_{NB}} + m\right) C_B \left(\frac{C_N(\bar{x},t)}{C_N(\bar{x},t) + K_N}\right) \quad (1)$$

where μ_{max} is the maximum specific growth rate, Y_{NB} and m are the yield and maintenance coefficients, respectively, and K_N is the half saturation concentration of the nutrient (N). The nutrient concentration field is governed by the reaction-diffusion-convection equation (Eq. 2)

$$\frac{\partial C_N(\bar{x},t)}{\partial t} = -r_N\left(C_N(\bar{x},t), C_B(\bar{x},t)\right) + D_N \sum_{i=1}^{3} \frac{\partial^2 C_N(\bar{x},t)}{\partial x_i^2} - \nabla \cdot (v C_N) \quad (2)$$

Here, D_N is the nutrient diffusivity, and v is the local fluid velocity. $C_N(\bar{x},t)$ is set to $C_{N,bulk}$ at the top surface, and to 0 at the substratum. Periodic boundary conditions are applied at the lateral boundaries.

Biomass growth

Consumption of nutrient leads to cell growth, and endogenous metabolism. Endogenous metabolism is assumed to be proportional to the biomass concentration. The leftover nutrient is utilized for cell growth at an efficiency Y_{NB}. The net accumulation of biomass is, given by:

$$\frac{\partial C_B(\bar{x},t)}{\partial t} = Y_{NB}\left[r_N\left(C_N(\bar{x},t), C_B(\bar{x},t)\right) - m C_B(\bar{x},t)\right] \quad (3)$$

Cell division

When the biomass of a cell increases to twice its native value it divides into two daughter cells. One daughter cell continues to occupy the same element as the mother cell, while the other is pushed into a cell-free element in the immediate, Moore neighborhood. For each cell, the Moore neighborhood, comprises of 26 cubical elements surrounding the central element. If multiple cell-free elements are available for occupation, one is chosen at random. On the other hand, if all elements in the Moore neighborhood are occupied by bacteria, an unoccupied element is identified at the nearest Chebyshev distance from the location of the mother cell. The occupancy statuses of elements are checked at successively larger Chebyshev distances (starting with a Chebyshev distance of 2, and moving outward, layer by layer), until an empty element is found. Each of the cells that lies between the mother cell and the closest cell-free element is then shifted by one grid element – away from the mother cell, and towards the empty element – creating a cell-free element in the Moore neighborhood of the mother cell. This newly created cell-free element is then occupied by the daughter cell, thereby ensuring that the daughter cell is always placed immediately next to the dividing bacterium [43].

Cell death

The nutrient uptake rate (R) is defined as the ratio of the nutrient uptake rate (r_N) to endogeneous metabolism (mC_B). There are three mechanisms by which a bacterium can die: (i) limited nutrient uptake rate (R), (ii) stay in the stationary phase for a predetermined number of hours (t_{SP}), and (iii) exposure to antibiotic. If $R > 1$, the bacterium exhibits net growth. On the other hand, for $R < 1$, the bacterium shows negative net growth, and is said to have entered the stationary phase. Bacteria die if R falls below a certain threshold (R_{min}). This is an attempt to account for bacterial death under nutrient starvation conditions. Bacteria also die if they have been in this growth-arrested phase for a pre-specified number of hours (t_{SP}). This is recorded with an individual based counter. If R is below 1 during one hour, the counter increases by one. However, a bacterium also has the possibility to recover if R increases above 1 before it dies. Consequently, if R is above 1 during one hour, the counter decreases by one. The counter can never be less than zero. Moreover, if the biofilm is subjected to antibiotic treatment, then cells die based on probability of killing by antibiotic which is a function of the rate of consumption of antibiotic (Eq. 13).

Cell detachment

We implement a simplified geometrical model of cell detachment governed by (i) localized cell death, and (ii) EPS formed as a consequence of quorum sensing. Cell detachment is determined by evaluating the connectivity of cells to the substratum. Within the biofilm, bacteria connect to the substratum either directly, or indirectly through a group of live bacteria in which at least one bacterium is directly bound to the substratum [51]. In addition to live bacteria, in QS^+ biofilms, cells can also continue to remain connected to the substratum via EPS. At the end of each time step, detachment events are recorded, and detached cells are removed from the domain.

Quorum Sensing

Every bacterium that engages in quorum sensing is allowed to switch randomly between the up-regulated, and the down-regulated state, at rates, dependent on the local autoinducer concentration$\left(C_A(\bar{x},t)\right)$ in the grid element. At time t = 0, all the bacteria are in the down-regulated state. The transition rate from the down-regulated to up-regulated state is given by

$$TR^{+} = \alpha \frac{C_A(\bar{x},t)}{1 + \gamma C_A(\bar{x},t)} \tag{4}$$

While, the transition rate between the up-regulated to down-regulated states is given by [52]

$$TR^{-} = \beta \frac{1}{1 + \gamma C_A(\bar{x},t)} \tag{5}$$

where α and β are the spontaneous up- and down-regulation rates, and γ is the transition constant.

Within a time interval of Δt, the probabilities of switching from one state to another are then given by

$$\begin{aligned} P_u &= (TR^{+})\Delta t \\ P_d &= (TR^{-})\Delta t \end{aligned} \tag{6}$$

where P_u is the probability of up-regulation, and P_d is the probability of down-regulation.

For each bacterium, at every time step, the simulation generates a random number (n_R) from a uniform distribution on the interval [0, 1]. If $P_u > n_R$, then the bacterium switches from the down-regulated state to an up-regulated state. On the other hand, if $P_d > n_R$, then the bacterium switches from the up-regulated to the down-regulated state.

Autoinducer Production and Transport

Up-regulated and down-regulated cells secrete autoinducer molecules at constant rates of $r_{A,u}$ and $r_{A,d}$, respectively.

$$r_A = \begin{cases} r_{A,u} \\ r_{A,d} \end{cases} \tag{7}$$

where $r_{A,u} > r_{A,d}$ (Table I). The secreted autoinducer is treated as a dissolved entity that is transported via diffusion and convection. The time evolution of autoinducer concentration within the biofilm is given by

$$\frac{\partial C_A(\bar{x},t)}{\partial t} = D_A \sum_{i=1}^{3} \frac{\partial^2 C_A(\bar{x},t)}{\partial {x_i}^2} + \frac{r_A}{\Delta V} - \nabla \cdot (vC_A) \tag{8}$$

where D_A is the autoinducer diffusivity, and ΔV is the element volume. Eq. 8 is subject to the Dirichlet boundary condition at the DBL ($C_{A,DBL} = 0$), and the no-flux condition at the substratum. Upregulated cells secrete autoinducer molecules and EPS at an enhanced rate, compared to their downregulated counterparts [52, 53]. In a feedback-like mechanism, enhanced

production of autoinducer by upregulated cells results in the upregulation of an increasing number of cells in the neighborhood.

EPS Production

EPS is treated as a discrete entity and is tracked individually in a manner similar to that of bacterial cells. Bacterial growth and EPS production are assumed to occur concurrently from nutrient that is leftover after maintenance has been accounted for. EPS is produced only by upregulated cells, at a rate given by

$$\frac{\partial C_E(\bar{x},t)}{\partial t} = Y_{NE}\left[r_N\left(C_N(\bar{x},t), C_B(\bar{x},t)\right) - mC_B(\bar{x},t)\right] \quad (9)$$

where, Y_{NE} is the yield coefficient for EPS, i.e. the efficiency with which unutilized nutrient is converted to EPS. EPS do not grow, die or consume nutrient, but they occupy space and undergo division. EPS division is handled similar to cell division described above, wherein daughter "EPS cells" are placed into the nearest element that does not contain EPS. The consumption of antibiotic by EPS is governed by Monod-like kinetics (Eq. 11). This is an attempt to account for the reaction-diffusion barrier to penetration by the antibiotic that EPS provides.

Diffusion and reaction of antibiotics

In select runs, the biofilm is subjected to a continuous antibiotic treatment for a duration of 24 h. The antibiotic concentration in the bulk fluid is held constant throughout the treatment period. As the antibiotic diffuses through the DBL, live bacterial cells and EPS consume the antibiotic in a Monod-like reaction [54]. The consumption of antibiotic by non-quorum sensing bacteria is assumed to be a function of the local antibiotic concentration and biomass concentrations, is given by Eq. (10)

$$r_{ab}\left(C_{ab}(\bar{x},t), C_B(\bar{x},t)\right) = \left(\frac{C_{ab}(\bar{x},t)}{C_{ab}(\bar{x},t)+K_{ab}}\right) K_{B\mathrm{Max}} C_B(\bar{x},t) \quad (10)$$

where $K_{B\mathrm{Max}}$ is the maximum specific reaction rate of antibiotic with respect to biomass, K_{ab} is the Monod half-saturation coefficient of antibiotic, and $C_{ab}(\bar{x},t) = C_{ab}(x,y,z,t)$ represents local antibiotic concentration in each grid element, at time point t. In QS^+ biofilms, the consumption of antibiotic by bacteria and EPS, is given by Eq. (11).

$$r_{ab}\left(C_{ab}(\bar{x},t), C_B(\bar{x},t)\right) = \left(\frac{C_{ab}(\bar{x},t)}{C_{ab}(\bar{x},t)+K_{ab}}\right) \left[K_{B\mathrm{Max}} C_B(\bar{x},t) + K_{E\mathrm{Max}} C_E(\bar{x},t)\right] \quad (11)$$

where K_{Emax} represents the maximum specific reaction rate of antibiotic by EPS, and C_E represents the EPS biomass. The dynamics of the antibiotic concentration field $C_{ab}(\bar{x},t)$ is given by the following reaction-diffusion equation:

$$\frac{\partial C_{ab}(\bar{x},t)}{\partial t} = -r_{ab}\left(C_{ab}(\bar{x},t), C_B(\bar{x},t)\right) + D_{ab}\sum_{i=1}^{3}\frac{\partial^2 C_{ab}(\bar{x},t)}{\partial x_i^2} - \nabla\cdot(vC_{ab}) \quad (12)$$

where D_{ab} is the antibiotic diffusivity, and v is the local fluid velocity.

The probability of cell death due to antibiotic consumption is given by:

$$P_{death} = \left(\frac{r_{ab}(\bar{x},t) - r_{Min}}{r_{Max} - r_{Min}}\right) \quad (13)$$

r_{Min} and r_{Max} are the rates of consumption of the antibiotic at minimum and maximum inhibitory concentrations of one bacterium, respectively. At each time step during treatment, a random number (n_R) is generated for each cell. If $P_{death} > n_R$, then the bacterium dies, and is removed from the simulation domain.

Bacterial heterogeneity based on growth rates

Cells within the biofilm are classified into three groups based on their growth rates: cells exhibiting (i) high (HGR), (ii) intermediate, and (iii) low growth rates (LGR). The growth rate of each cell is evaluated as the change in biomass over a period of 4 h. Growth rates vary from ~10 to ~10,000 $gm^{-3}h^{-1}$. After 64 h of growth (in the absence of antibiotic treatment), cells are sorted from highest to the lowest growth rates. The top 10% of the cell population is classified as HGR, and the bottom 10% as LGR. This percentage of HGR is in agreement with experimental observations that suggest that the proportion of active bacteria in biofilms is range from ~5-35% [55, 56]. Using this methodology, the threshold growth rate above which cells ae classified as HGR is set to 6000 $gm^{-3}h^{-1}$, and that below which cells are classified as LGR is set to 425 $gm^{-3}h^{-1}$.

Model Simulation and Numerical Scheme

The simulation represents a time march in which the occupancy states of each grid element is updated at discrete time steps of 1 h. Previous work analyzing the kinetics of the switching process from the vegetative state to the competent (EPS producing) state of *Bacillus subtilis* (*B. subtilis*) has shown that the duration of the switching period was 1.4 ± 0.3 h [57]. In addition, analysis of *B. subtilis* at the interface between the culture medium and air indicates that bacteria switch from the motile to the matrix-producing phenotype (downregulated to upregulated) between 10 min to 1h [58]. We use a multiscale integration approach with two distinct time scales: (i) cellular processes (biomass growth (Eq. 3), EPS production (Eq. 9), switching between up- and down-regulated states (Eq. 6), death by antibiotic (Eq. 13), cell division, and detachment) are monitored every 1 h, and (ii) within this "outer" time loop, concentrations of dissolved entities (nutrient (Eq. 2), autoinducer (Eq. 8), and antibiotic (Eq. 12)) are tracked by solving the diffusion-convection equations at a finer time resolution of $1x10^{-6}$ h. Numerical solutions to the diffusion-convection equations are obtained using a second-order Forward-Time Central-Space scheme. Periodic boundary conditions are applied in the horizontal directions, and the Dirichlet boundary condition is imposed in the vertical direction. The Java programming

language is used since it provides a convenient object-oriented framework that is well-suited for the individual based model described here.

The parameter values used in the model are summarized in Table I.

Results

Biofilm growth dynamics in response to antibiotic treatment

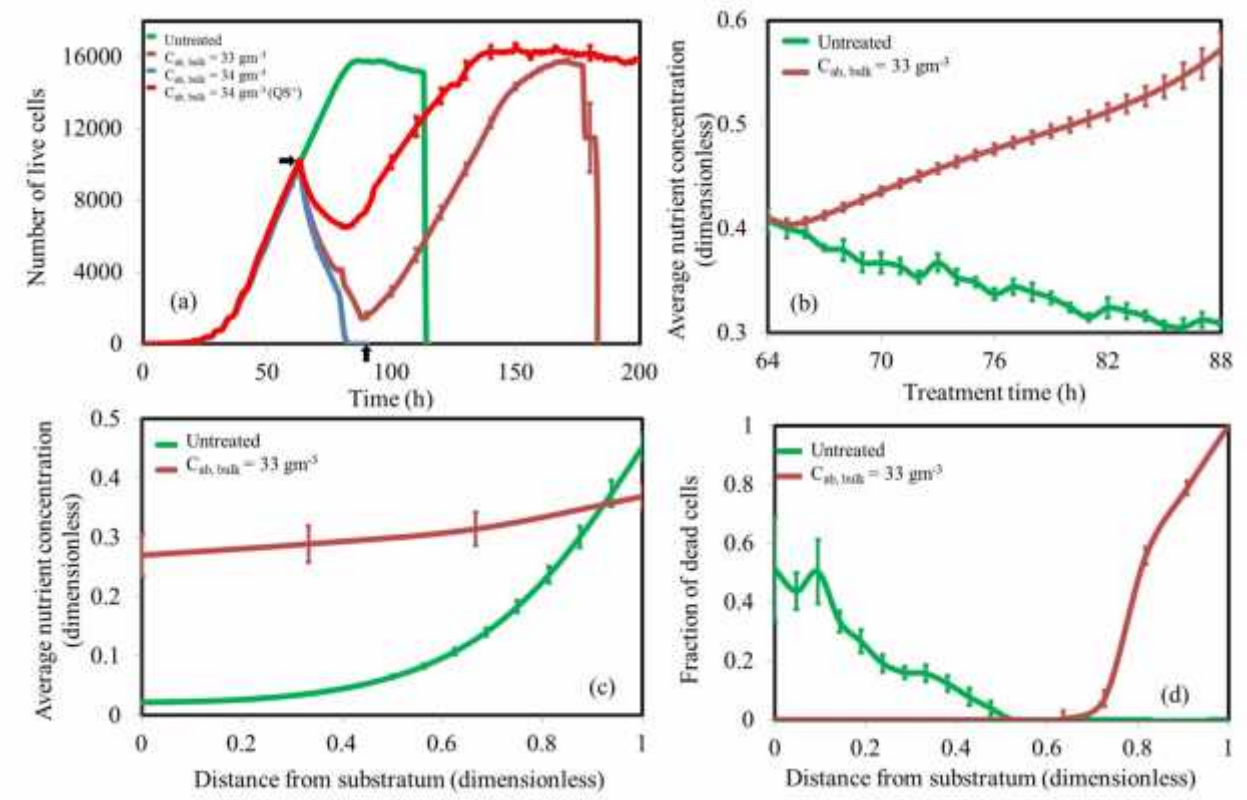

Fig. 1. Growth dynamics of QS$^-$ and QS$^+$ biofilms in the absence and presence of antibiotic treatment. The number of live cells as a function of time for $C_{N,bulk} = 4\,gm^{-3}$ for the untreated QS$^-$ biofilm (green), and when subjected to a continuous 24h (64-88 h) treatment of sub-MBEC ($C_{ab,bulk} = 33\,gm^{-3}$, red), and MBEC ($C_{ab,bulk} = 34\,gm^{-3}$, blue); the QS$^+$ biofilm is subjected to $C_{ab,bulk} = 34\,gm^{-3}$ (orange) (a), comparisons of average nutrient concentration (b), spatial distribution of average nutrient concentration (c) and spatial distribution of fraction of dead cells (d) for the QS$^-$ biofilm subjected to sub-MBEC and the untreated biofilm. Data in panels (c) and (d) are reported at 88 h, the time point at which treatment stops. The arrows in panel (a) represent – initial (64 h) and end (84 h) time points of antibiotic treatment. Data represent mean ± standard error of mean (SEM) of four replicate simulations.

We simulated the growth dynamics of a bacterial biofilm over a period of 200 h, in the presence and absence of QS. In select runs, the biofilm was subjected to a continuous antimicrobial treatment ($C_{ab,bulk}$ ranging from 15 to 60 gm^{-3}) for duration of 24 h, initiated after 64 h of growth (cell number ~10,000). Whereas subjecting the biofilm to $C_{ab,bulk}$ of 34 gm^{-3} resulted in complete removal after 21 ± 0.5 h of treatment (Fig. 1a), a slightly lower antibiotic concentration (33 gm^{-3}) was insufficient to eradicate the biofilm. Interestingly, biofilms treated with sub-MBEC ($C_{ab,bulk}$ of 33 gm^{-3}) exhibited a prolonged lifetime compared to even the

407 untreated biofilms, with the former sloughing off at 113 ± 0.5 h while the latter at 184 ± 2.7 h
408 (Fig. 1a). This is in line with the experimental observation that sub-MBEC treatment enhances
409 biofilm formation [59]. The average nutrient concentration within the sub-MBEC-treated
410 biofilm increased monotonically with time, and was higher compared to the untreated one (Fig.
411 1b). This is a consequence of the fact that antibiotic-induced cell death in the sub-MBEC-
412 treated biofilm causes the live cell number – and hence, the overall nutrient consumption – to
413 decrease. In contrast, bacterial biomass in the untreated biofilm increases with time, resulting in
414 increased nutrient consumption and reduced average nutrient concentration compared to the sub-
415 MBEC-treated biofilm. The spatial distribution of nutrient concentration (measured as a
416 function of the distance from the substratum) shows that nutrient penetration to the lower layers
417 in the untreated biofilm was lower compared to the treated biofilm (Fig. 1c). This, in turn,
418 causes cell death to occur near the bottom for the untreated biofilm, subsequently leading to
419 sloughing (Fig. 1d). These findings are in agreement with experimental results showing that
420 localized nutrient starvation is an environmental cue for the sloughing of biofilms [60]. In
421 contrast, cell death was restricted to the top layers in the sub-MBEC-treated biofilm (Fig.
422 1d). In agreement with experimental observations, sub-MBEC-treatment does not fully
423 eradicate bacteria during the treatment phase [61], and biofilm thickness was restored to pre-
424 treatment levels within 24 h after exposure to the antibiotic.
425
426 MBEC for the QS^+ biofilm was 51 gm^{-3}, and was significantly higher than that for QS^-.
427 Comparing responses of the QS^- and QS^+ biofilms when subjected to a bulk antibiotic
428 concentration of 34 gm^{-3} showed that whereas there was no significant difference in the viable
429 cell counts for the first 8 hours of treatment, the live cell number for the QS^+ biofilm reduced at
430 a lower rate for the rest of the treatment (Fig. 1a).
431
432

Comparison of responses to MBEC- and sub-MBEC-treatments

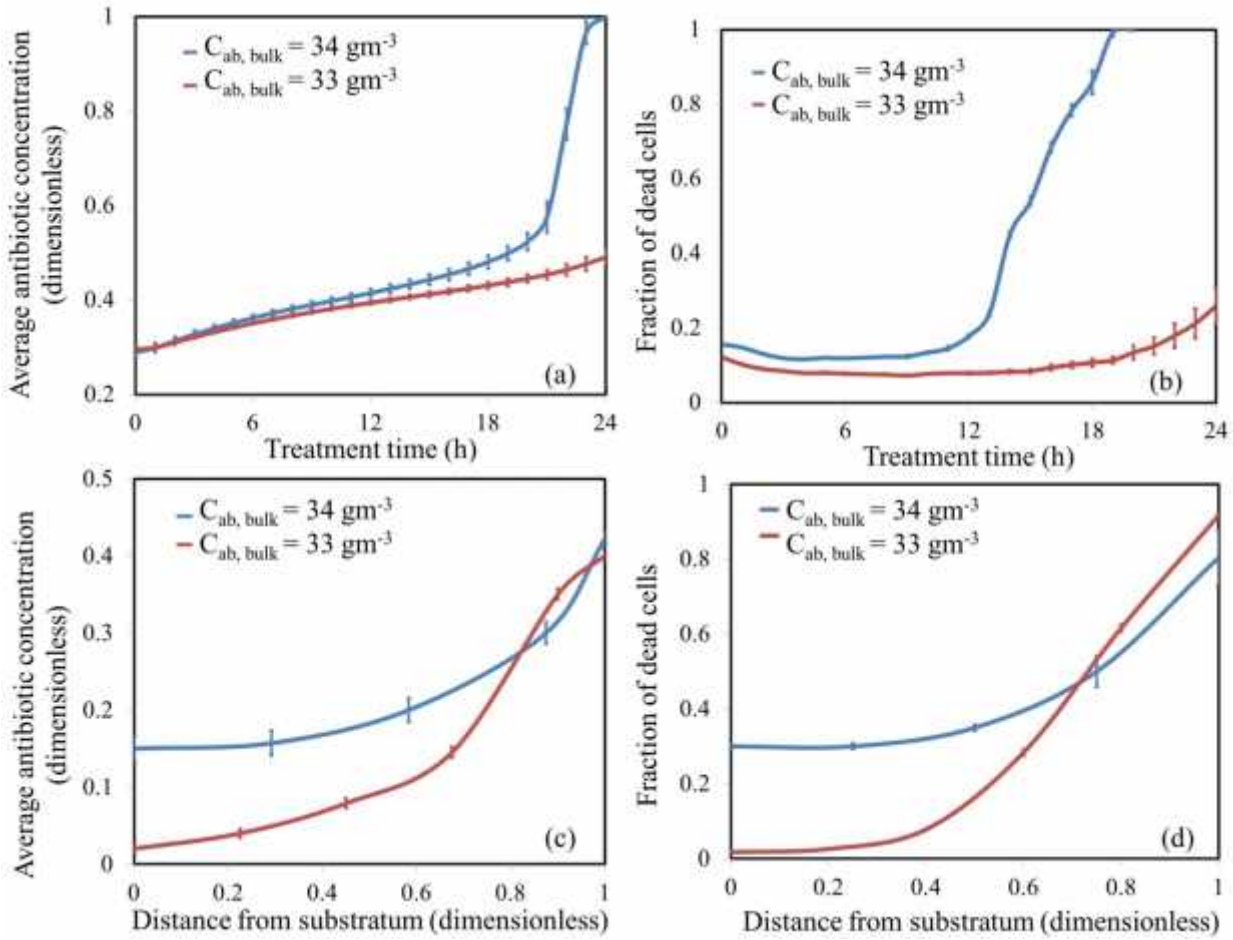

Fig. 2. **Response of the biofilm to MBEC and sub-MBEC treatments.** The average antibiotic concentration (a) and fraction of dead cells (b) as a function of time, upon treatment with MBEC (blue) and sub-MBEC (red). Spatial profiles for antibiotic concentration (c), and fraction of dead cells (d) after 16 h of treatment for the MBEC-treated (blue) and sub-MBEC-treated (red) biofilms. Data represent mean ± standard error of mean (SEM) of four replicate simulations.

To investigate the dramatically different responses of the QS$^-$ biofilms subjected to two slightly different antibiotic concentrations (MBEC and sub-MBEC), we tracked the temporal variation in the average antibiotic concentrations within the biofilms. A small difference in the bulk antibiotic concentrations (1 gm^{-3}) was amplified to a much larger difference in average antibiotic concentrations within the biofilms; this difference was more pronounced at higher time points (after ~12 h of treatment) (Fig. 2a). This, in turn, led to higher cell death events in MBEC-treated biofilms compared to the ones treated with sub-MBEC (Fig. 2b). Under these conditions (after ~12 h of treatment), antibiotic penetration to the lower layers was more effective in the biofilm treated with MBEC compared to the one treated with sub-MBEC (Fig. 2c). For instance, after 16 h of treatment, the average antibiotic concentration at the substratum of the biofilm exposed to MBEC was ~7.5 times that of the biofilm treated with sub-MBEC (Fig. 2c). This marked difference in local antibiotic concentrations in the lower regions of the biofilm

resulted in significantly higher death events for the MBEC-treated biofilm compared to the biofilm treated with sub-MBEC (Fig. 2d). Whereas ~30% of the cells in the lowest layer died when the biofilm was subjected to MBEC, negligible cell death (~2%) occurred near the substratum of the sub-MBEC-treated biofilm (Fig. 2d). This difference in the fraction of dead cells at the bottom layers of the biofilm was observed at all treatment time points, ultimately leading to the eradication of the MBEC-treated biofilm. Similar trends were observed for the QS+ biofilm upon MBEC- (51 gm^{-3}) and sub-MBEC (50 gm^{-3}) treatments (data not shown).

Correlation between cellular metabolism rates and antibiotic-induced death

Biofilms comprise of bacterial cells in a wide range of physiological states, resulting in a spatially heterogeneous system. To investigate the influence of this spatial heterogeneity on the response of the biofilm to MBEC- and sub-MBEC treatments, we categorized live cells into three groups based on their growth rates: (i) metabolically active cells, exhibiting high growth rates (HGR), (ii) intermediate, and (iii) dormant cells, exhibiting low growth rates (LGR). There was a strong correlation between dead cells and HGR-cells in the presence of antibiotic treatment. On an average, during treatment, 59.79 ± 6.1% of HGR died at any given time step. On the other hand, LGR-cells were less susceptible to killing by antibiotic (~ 0.001%). In stark contrast, in the absence of antibiotic treatment, there was a strong correlation between dead cells and LGR-cells, with 34.15 ± 2.8% of LGR dying on an average at any given time step. Under these conditions, cell death occurred predominantly due to nutrient starvation at later time points (80 h onwards). The number of dead HGR-cells was negligible in the untreated biofilm.

Spatial distribution of heterogeneous subpopulations in biofilms during treatment

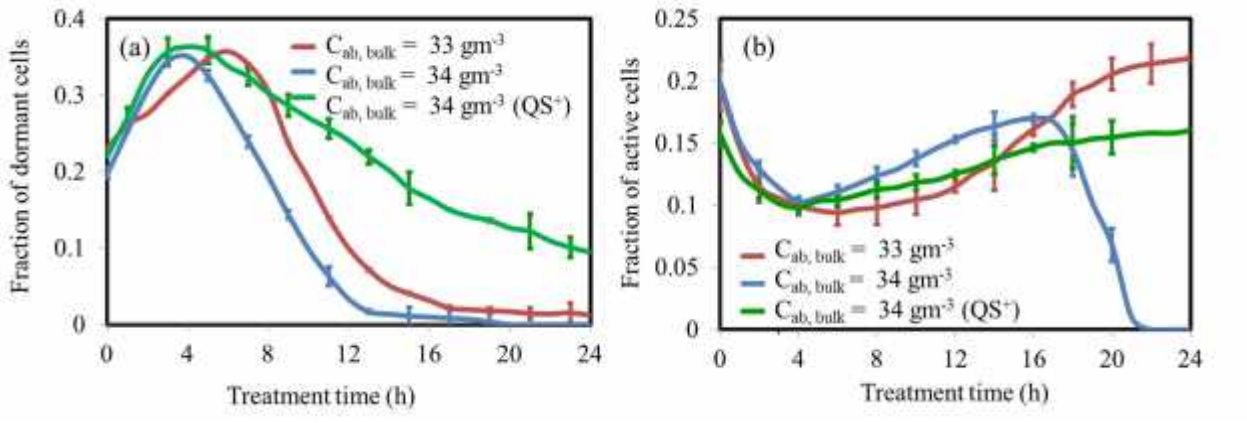

Fig. 3. Growth dynamics of subpopulations in the presence of antibiotic. Comparison of fraction of dormant cells (a), fraction of metabolically active cells (b) as a function of time for $C_{N,bulk}$ = 4 gm^{-3}. QS$^-$ biofilms treated with MBEC (blue) and sub-MBEC (red), and QS$^+$ biofilm subjected to $C_{ab,bulk}$ of 34 gm^{-3} (green). Data represent mean ± standard error of mean (SEM) of four replicate simulations.

We tracked the dynamics of the distinct growth-rate-based cell subpopulations in QS$^-$ and QS$^+$ biofilms in response to antibiotic treatment. Based on the fraction of HGR- and LGR-cells, three distinct phases were observed during 24 h of continuous antibiotic treatment (Figs. 3a and 3b). In the first phase that lasted ~4h, the total biomass reduced dramatically (~40% reduction). In this phase, the fraction of dormant cells increased with time, reaching a peak after 4h of treatment (Fig. 3a). On the other hand, the subpopulation of active cells decreased with time (Fig. 3b). After 4 h, the antibiotic consumption rates by dormant cells in the MBEC-treated biofilms were ~17 times higher compared to those of active cells (50.5 ± 9.4 gm^{-3} h^{-1} for dormant cells, versus 850.5 ± 65.4 gm^{-3} h^{-1} for active cells). This indicates that metabolically active cells at the distal edge of the biofilm act as a reaction-diffusion barrier, thereby reducing antibiotic penetration to the LGR-cells near the substratum. This results in lower antibiotic uptake rates by the LGR-cells, allowing them to survive antibiotic treatment. The second phase lasted for ~8h, and was characterized by a decrease in the number of dormant cells (Fig. 3a). For the biofilm treated with MBEC, phases I and II were qualitatively similar to those observed for sub-MBEC treated biofilm. However phase II is delayed and prolonged in the biofilms treated with sub-MBEC (~5 h to 18 h) in comparison with MBEC-treated biofilms (4h to 12 h). The third phase was characterized by the complete eradication of the MBEC-treated biofilm. In contrast, the sub-MBEC-treated biofilm survived in phase III. More importantly, the fraction of active cells in the third phase of sub-MBEC treatment increased, resulting in the regrowth of the biofilm after the termination of antibiotic treatment.

The QS$^+$ biofilm survived treatment at $C_{ab,bulk}$ of 34 gm^{-3}. In contrast to the QS$^-$ biofilm, the fraction of dormant cells increased monotonically in the third phase of QS$^+$ biofilms (Fig. 3a). This could be a direct consequence of the increased viable cell number during treatment (Fig. 1a), resulting in reduced nutrient availability in the lower regions of the biofilm. This starvation may lead to lower metabolic activity. Although both QS$^-$ and QS$^+$ biofilm survived treatment

with 33 gm^{-3}, the mechanisms of survival appear to be different. Whereas the QS^- biofilm survives by rapidly transforming the metabolically inactive cells into active ones, the survival of the QS^+ biofilm is a consequence of reduced exposure of the dormant cells to antibiotic.

Spatial distribution of growth rates

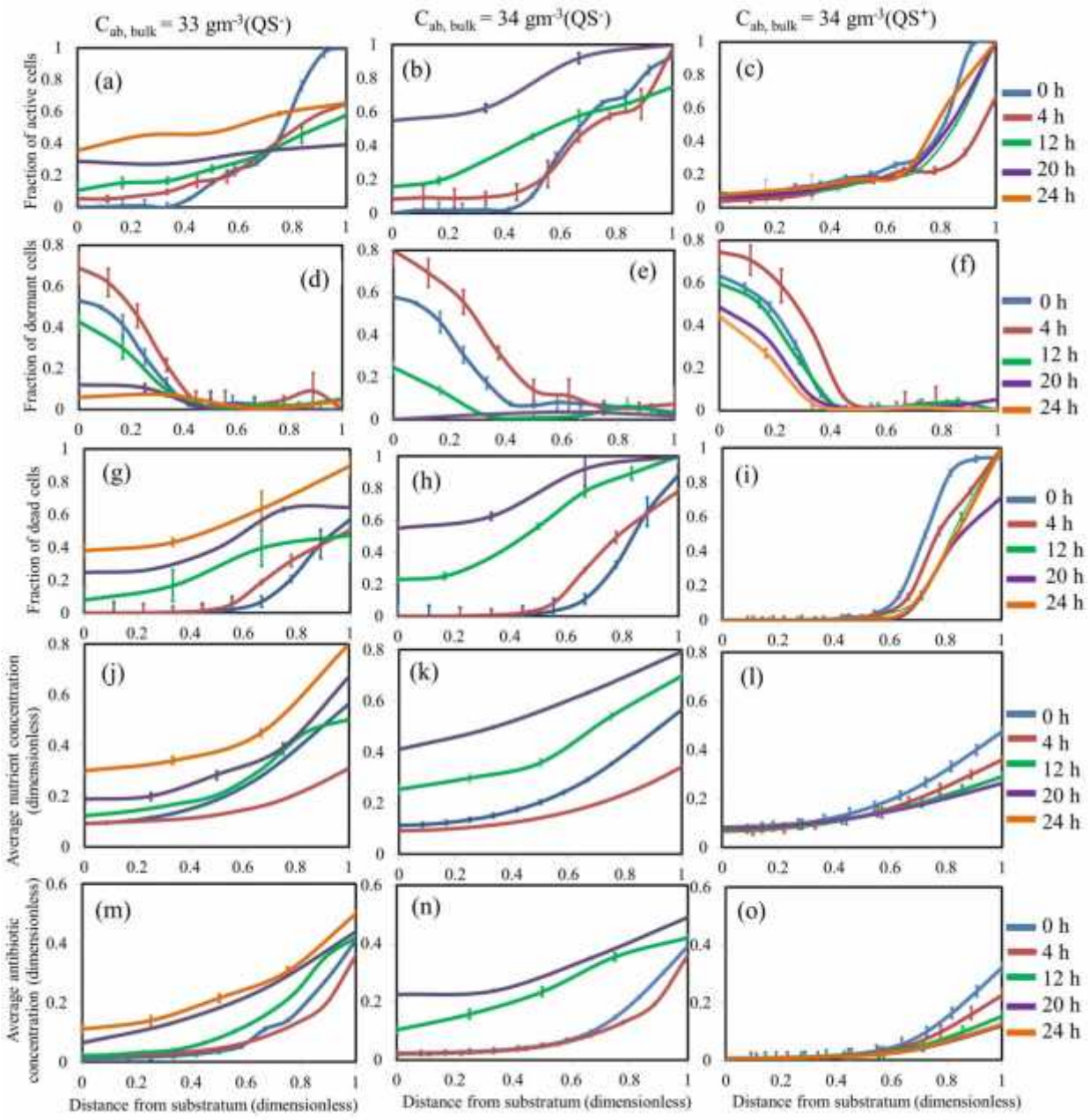

Fig. 4. Spatial heterogeneity in treated QS$^-$ and QS$^+$ biofilm. Comparison of sub-MBEC (panels a, d, g, j, and m) and MBEC-treated QS$^-$ biofilms (panels b, e, h, k, n) and MBEC-treated QS$^+$ biofilms (panels c, f, i, l, o) at different time points during 24 h treatment period. The spatial distribution of the fraction of dormant cells (panels a-c), active cells (panels d-f), and dead cells (panels g-i), local nutrient (panels j-l), and antibiotic concentrations (m-o). Data represent mean ± standard error of mean (SEM) of four replicate simulations.

To investigate the biophysical mechanisms for the formation of surviving cell pockets within the antibiotic-treated biofilm, we tracked the growth rates of individual cells, the distribution of

dead cells, and local nutrient and antibiotic concentrations as a function of their position within the biofilm. Prior to exposure to antibiotics (64 h of growth), a majority of the metabolically active cells are located at the upper layers (Figs. 4a-c), and dormant cells are localized at the lower layers (Figs. 4d-f). Upon initiation of treatment, cells at the biofilm-bulk liquid interphase are exposed to the antibiotic, resulting in cell death; cell death in the lower regions during this time period is negligible (Figs. 4g-i). Because of the consumption of antibiotic by active cells in the top layers, antibiotic penetration to lower layers is reduced (Figs. 4m-o). Cells in the lower layers are, thus, able to survive the initial period of treatment. Consequently, the fraction of dormant cells increases near the substratum and active cells decreased at the top (Figs. 4d-f). At the end of phase I (4-6 h of treatment), nutrient penetration increased to the interior of the biofilm (Figs. 4j, 4k). Subsequently, dormant cells located in the lower layers of the biofilm had improved nutrient accessibility, resulting in increased growth rates. This, in turn, results in the transformation of inactive cells to the metabolically active state. This is validated by the observation that the fraction of dormant cells decreases and the fraction of active cells increases near the substratum over time (Figs. 4a, 4b, 4d, 4e).

Antibiotic penetration to the lower layers in the MBEC-treated biofilm was higher compared to that in the sub-MBEC-treated biofilm (Fig. 4m, 4n). In the surviving QS^+ biofilm (exposed to $C_{ab,bulk}$ of 34 gm^{-3}), even the topmost bacterial cell was exposed to a local antibiotic concentration that was always less than 30% of the bulk value (Fig. 4o). This is a direct consequence of the sequestration of the antibiotic by the cell-devoid layer of EPS that forms at the distal edge of the biofilm (Fig. 5a). In stark contrast, in the QS^- biofilm subjected to treatment with MBEC, the local antibiotic concentration even at the substratum increased with time, reaching a maximum value of 22.5% of the bulk antibiotic concentration (after 20 h of treatment). Under these conditions, the local antibiotic concentration to which the topmost cell in the biofilm was exposed was as high as 50%.

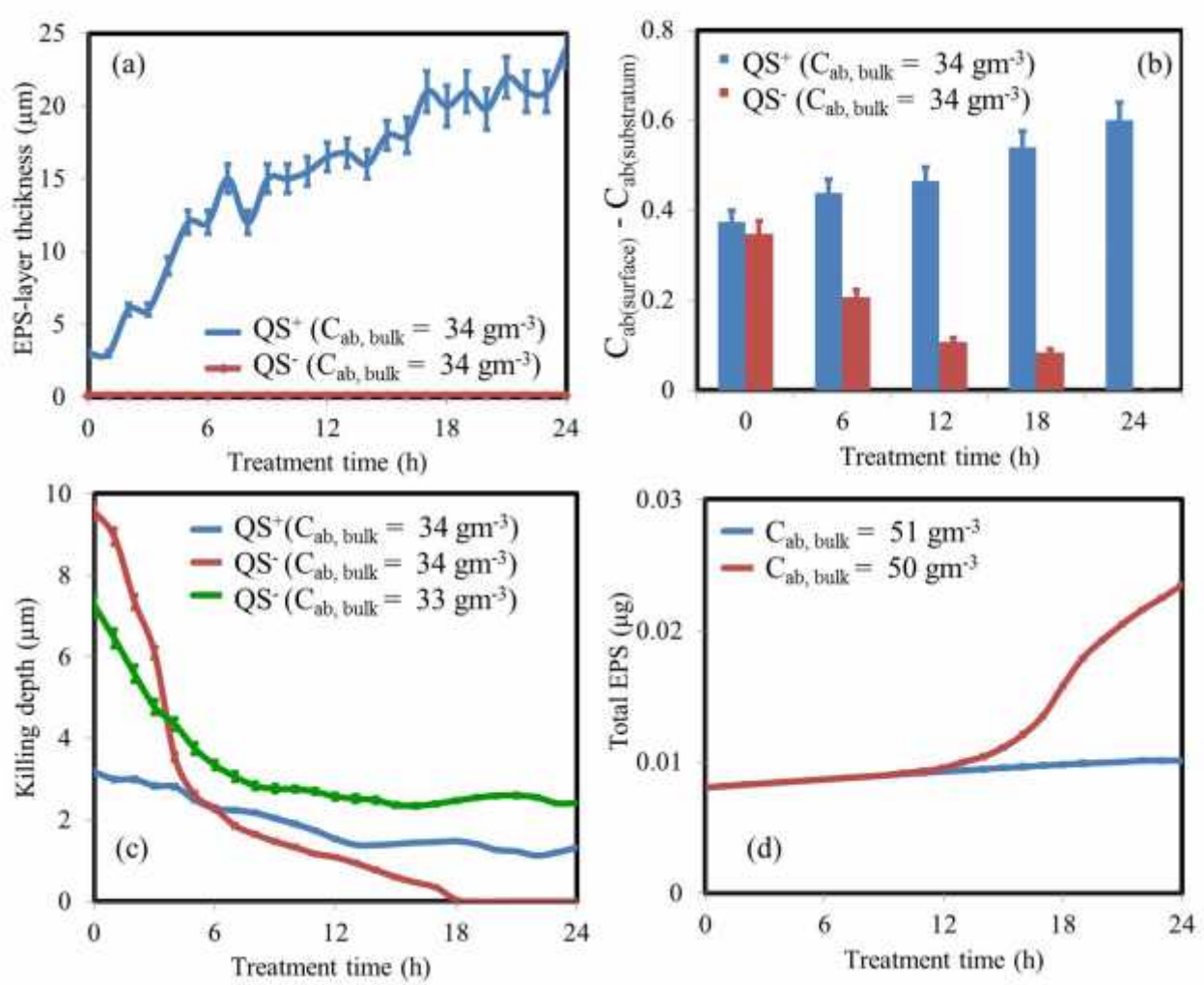

Fig. 5. Comparison of the response of QS^+ and QS^- biofilms to antibiotic treatment. Thickness of the cell-devoid layer of EPS at the top of the biofilm plotted as a function of treatment time (a), the difference between the average antibiotic concentrations at the biofilm surface and the substratum for QS^+ (blue) and QS^- (red) biofilms subjected to $C_{ab,bulk}$ of 34 gm^{-3} (b), the average killing depth for QS^+ (blue) and QS- biofilms subjected to $C_{ab,bulk}$ of 34 gm^{-3} (red) and $C_{ab,bulk}$ of 33 gm^{-3} (green) (c), and the total EPS produced for QS+ biofilms subjected to $C_{ab,bulk}$ of 50 gm^{-3} (red) and $C_{ab,bulk}$ of 51 gm^{-3} (blue) (d). Data represent mean ± standard error of mean (SEM) of four replicate simulations.

Next, we compared the responses of the QS^- (MBEC = 33 gm^{-3}) and QS^+ (MBEC = 51 gm^{-3}) biofilms subjected to $C_{ab,bulk}$ of 34 gm^{-3}. A cell-devoid layer of EPS is formed at the top of the QS^+ biofilm, and the thickness of this layer increases as treatment proceeds (Fig. 5a). The extent of antibiotic penetration was quantified as the difference between the average antibiotic concentration at the surface of the biofilm and that at the substratum; lower the difference,

higher the extent of penetration. Antibiotic penetration in the QS^+ biofilm was significantly lower compared to that in the QS^- biofilm (Fig. 5b), indicating that EPS sequesters antibiotic, thereby lowering the local concentrations in the interior of the biofilm. The largest distance from the surface of the biofilm at which antibiotic-induced cell death occurs was termed the killing depth. In agreement with the observation of fig. 5b, the killing depth for the QS^- biofilms was higher than that for the QS^+ biofilm. The killing depth decreased monotonically with time for both QS^- and QS^+ biofilms as the biofilm thickness reduced. Interestingly, the QS^+ biofilm subjected to a sub-MBEC treatment ($C_{ab\,bulk}$ of 51 gm^{-3}) exhibited enhanced EPS production compared to that when subjected to the MBEC treatment (Fig. 5d).

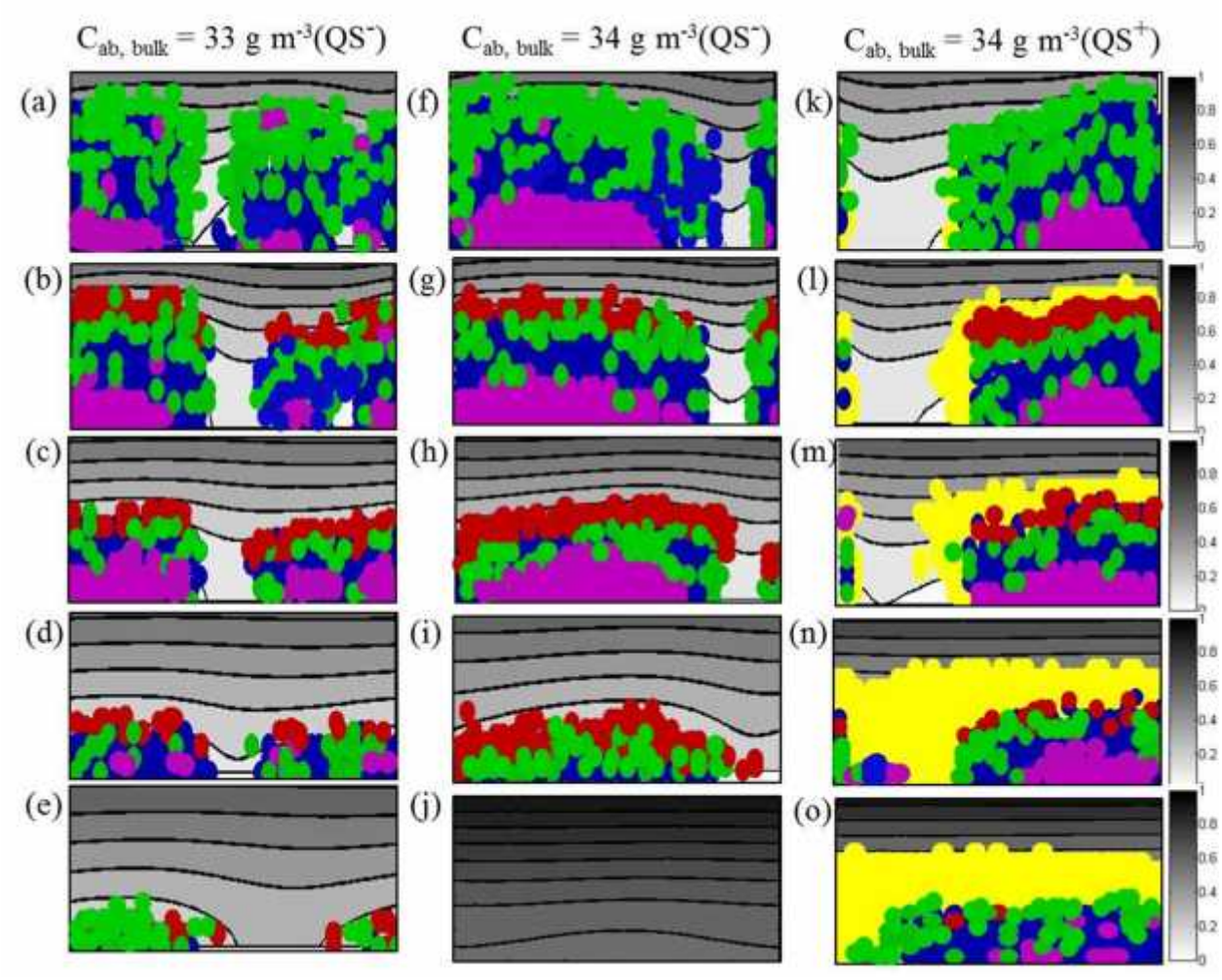

Fig. 6. **QS$^-$ Biofilms treated with sub-MBEC (a, b, c, d, e) and MBEC (f, g, h, i, j), and QS$^+$ biofilms treated with MBEC (k, l, m, n, o).** Visualization of 2D cross-sections showing high growth rate (green), intermediate growth rate cells (cyan), low-growth rate (blue), and locations of cell death (red), of the $C_{N,bulk}$ = 4 gm^{-3} biofilm after 0 h, 1 h, 4 h, 20 h, and 24 h of antibiotic introduction. The yellow color represents EPS in QS$^+$ biofilm. The isolines show the antibiotic concentration distribution.

Fig. 6 shows representative biofilm cross-sections at various stages of the response, illustrating the formation of surviving cell pockets within antibiotic-treated QS$^-$ and QS$^+$ biofilms. After the first hour of treatment (panels 6a, 6e, and 6i), dormant cells (pink) were localized in the interior of the biofilm, and were surrounded by layers of cells exhibiting high (green), and intermediate (blue) growth rates. Antibiotic-induced cell death events (red) occurred at and near the biofilm-bulk liquid interface. For the QS$^-$ biofilms, thickness reduces as treatment continues, resulting in increased nutrient availability in the bottom layers. This causes the slow-growing (pink) cells to transform into cells with intermediate- (blue) and high- (green) growth rates. This is evident by the diminishing population of slow-growing cells in panels (6b), (6c), (6g), and (6h). For the

QS^+ biofilm, antibiotic-induced cell death events at the top resulted in the formation of a thin cell-devoid layer of EPS (yellow). This result is in agreement with experimental investigations that indicate that EPS was most abundant at the upper layers of the biofilm [62]. Antibiotic penetration was hindered by an interaction with the matrix of EPS, and results in the protection of bacterial cells in the lower layers. These results are in agreement with previous experimental investigation that suggests that the production of EPS by QS, and the subsequent accumulation in the upper regions of the biofilm, plays a key role in biofilm resistance [41].

Conclusions

Although bacteria are traditionally investigated as planktonic entities, they predominantly occur as sessile, substratum-associated biofilms. Bacteria associated with the biofilm mode of growth are more resistant to antibiotics, compared to their planktonic counterparts. Several hypotheses have been proposed to explain this resistance including upregulation of virulence factors, formation of persister cells, genetic manipulations, slow penetration of the antibiotic, and the presence of dormant, slow-growing cells. Most of these mechanisms involve antibiotic resistance at the single-cell level, and do not account for the effects of intercellular population dynamics. Physical mechanisms of resistance like retarded penetration of the antibiotic may be a factor in the early stages of treatment, but as treatment proceeds and cells at the top die, antibiotic penetration to the lower layers increases. Hence, retarded penetration of the antibiotic may not be a sufficient explanation as a protecting mechanism in biofilms.

Biofilms comprise of physiologically distinct subpopulations of cells exhibiting varying growth rates, due in part to their adaptation to local environmental conditions. We have previously characterized this spatial heterogeneity in biofilms [43]. Interestingly, response of biofilms to an antibiotic challenge is also heterogeneous, with only certain subpopulations becoming resistant while the rest of the biofilm remains sensitive. Our goal was to investigate the influence of the biophysical features of the biofilm mode of growth on antibiotic resistance, when each individual cell itself is not necessarily tolerant to antibiotics. This may help delineate the effect of population dynamics on the antibiotic resistance in biofilms. We also wished to correlate the inherent spatial heterogeneity of biofilms at the cellular level to their heterogeneous response to treatment. Consequently, in our model, each bacterium was modeled as an independent entity, allowing us to monitor structural and chemical heterogeneities in the biofilm and in its response to treatment as a function of time and space.

We first estimated the minimum antibiotic concentration required to eradicate biofilms in our simulations. This allowed us to identify the largest antibiotic concentration that the biofilm is able to survive. These are the conditions we used to further investigate mechanisms of antibiotic resistance in biofilms. Small differences in the bulk antibiotic concentrations were amplified into much larger differences in local antibiotic concentrations to which cells are exposed. When subjected to MBEC and sub-MBEC treatments, the local antibiotic concentration near the substratum for the MBEC-treated biofilm was ~13 times higher compared to that for the sub-MBEC-treated biofilm, although the difference in the bulk antibiotic concentrations was small (1 gm^{-3}). QS^- (non-EPS producing) biofilms, subjected to an antibiotic challenge, responded by increasing the rate of transformation of dormant cells into faster growing, metabolically active cells. In contrast, QS^+ biofilms responded by enhancing the rate

of EPS production. Overall, insights into these biophysical mechanisms associated with the biofilm mode of growth may pave the way for novel therapeutic strategies to combat the antibiotic resistance of biofilms.

Acknowledgments

This work was supported by the Start-Up Research Grant (No. SB/YS/LS-210/2013), Science and Engineering Research Board, India.

References

1. Donlan, R.M., *Biofilms: microbial life on surfaces.* Emerg Infect Dis, 2002. **8**(9): p. 881-90. 10.3201/eid0809.020063
2. Flemming, H.C., et al., *Biofilms: an emergent form of bacterial life.* Nat Rev Microbiol, 2016. **14**(9): p. 563-75. 10.1038/nrmicro.2016.94
3. Leid, J.G., *Bacterial Biofilms Resist Key Host Defenses.* Microbe 2009. **4**(Number 2,): p. 66-70.
4. Hathroubi, S., et al., *Biofilms: Microbial Shelters Against Antibiotics.* Microb Drug Resist, 2017. **23**(2): p. 147-156. 10.1089/mdr.2016.0087
5. Hall, C.W. and T.F. Mah, *Molecular mechanisms of biofilm-based antibiotic resistance and tolerance in pathogenic bacteria.* FEMS Microbiol Rev, 2017. **41**(3): p. 276-301. 10.1093/femsre/fux010
6. Gupta, K., et al., *Antimicrobial tolerance of Pseudomonas aeruginosa biofilms is activated during an early developmental stage and requires the two-component hybrid SagS.* J Bacteriol, 2013. **195**(21): p. 4975-87. 10.1128/JB.00732-13
7. He, X. and J. Ahn, *Differential gene expression in planktonic and biofilm cells of multiple antibiotic-resistant Salmonella Typhimurium and Staphylococcus aureus.* FEMS Microbiol Lett, 2011. **325**(2): p. 180-8. 10.1111/j.1574-6968.2011.02429.x
8. Wood, T.K., S.J. Knabel, and B.W. Kwan, *Bacterial persister cell formation and dormancy.* Appl Environ Microbiol, 2013. **79**(23): p. 7116-21. 10.1128/AEM.02636-13
9. Pamp, S.J., et al., *Tolerance to the antimicrobial peptide colistin in Pseudomonas aeruginosa biofilms is linked to metabolically active cells, and depends on the pmr and mexAB-oprM genes.* Mol Microbiol, 2008. **68**(1): p. 223-40. 10.1111/j.1365-2958.2008.06152.x
10. Beaudoin, T., et al., *The biofilm-specific antibiotic resistance gene ndvB is important for expression of ethanol oxidation genes in Pseudomonas aeruginosa biofilms.* J Bacteriol, 2012. **194**(12): p. 3128-36. 10.1128/JB.06178-11
11. Lewis, K., *Multidrug tolerance of biofilms and persister cells.* Curr Top Microbiol Immunol, 2008. **322**: p. 107-31.
12. LaFleur, M.D., C.A. Kumamoto, and K. Lewis, *Candida albicans biofilms produce antifungal-tolerant persister cells.* Antimicrob Agents Chemother, 2006. **50**(11): p. 3839-46. 10.1128/AAC.00684-06
13. Sultana, S.T., D.R. Call, and H. Beyenal, *Eradication of Pseudomonas aeruginosa biofilms and persister cells using an electrochemical scaffold and enhanced antibiotic susceptibility.* npj Biofilms and Microbiomes, 2016. **2**(1): p. 2. 10.1038/s41522-016-0003-0
14. Gilbert, P., et al., *The physiology and collective recalcitrance of microbial biofilm communities.* Adv Microb Physiol, 2002. **46**: p. 202-56.

15. Kostakioti, M., M. Hadjifrangiskou, and S.J. Hultgren, *Bacterial biofilms: development, dispersal, and therapeutic strategies in the dawn of the postantibiotic era.* Cold Spring Harb Perspect Med, 2013. **3**(4): p. a010306. 10.1101/cshperspect.a010306
16. Stewart, P.S. and J.W. Costerton, *Antibiotic resistance of bacteria in biofilms.* Lancet, 2001. **358**(9276): p. 135-8.
17. Stewart, P.S. and M.J. Franklin, *Physiological heterogeneity in biofilms.* Nat Rev Microbiol, 2008. **6**(3): p. 199-210. 10.1038/nrmicro1838
18. Mah, T.F. and G.A. O'Toole, *Mechanisms of biofilm resistance to antimicrobial agents.* Trends Microbiol, 2001. **9**(1): p. 34-9.
19. de la Fuente-Nunez, C., et al., *Bacterial biofilm development as a multicellular adaptation: antibiotic resistance and new therapeutic strategies.* Curr Opin Microbiol, 2013. **16**(5): p. 580-9. 10.1016/j.mib.2013.06.013
20. Yang, L., et al., *In situ growth rates and biofilm development of Pseudomonas aeruginosa populations in chronic lung infections.* J Bacteriol, 2008. **190**(8): p. 2767-76. 10.1128/JB.01581-07
21. Williamson, K.S., et al., *Heterogeneity in Pseudomonas aeruginosa biofilms includes expression of ribosome hibernation factors in the antibiotic-tolerant subpopulation and hypoxia-induced stress response in the metabolically active population.* J Bacteriol, 2012. **194**(8): p. 2062-73. 10.1128/JB.00022-12
22. Haagensen, J.A., et al., *Differentiation and distribution of colistin- and sodium dodecyl sulfate-tolerant cells in Pseudomonas aeruginosa biofilms.* J Bacteriol, 2007. **189**(1): p. 28-37. 10.1128/JB.00720-06
23. Walters, M.C., 3rd, et al., *Contributions of antibiotic penetration, oxygen limitation, and low metabolic activity to tolerance of Pseudomonas aeruginosa biofilms to ciprofloxacin and tobramycin.* Antimicrob Agents Chemother, 2003. **47**(1): p. 317-23.
24. Kolpen, M., et al., *Increased bactericidal activity of colistin on Pseudomonas aeruginosa biofilms in anaerobic conditions.* Pathog Dis, 2016. **74**(1): p. ftv086. 10.1093/femspd/ftv086
25. Borriello, G., et al., *Oxygen limitation contributes to antibiotic tolerance of Pseudomonas aeruginosa in biofilms.* Antimicrob Agents Chemother, 2004. **48**(7): p. 2659-64. 10.1128/AAC.48.7.2659-2664.2004
26. Mulcahy, L.R., V.M. Isabella, and K. Lewis, *Pseudomonas aeruginosa biofilms in disease.* Microb Ecol, 2014. **68**(1): p. 1-12. 10.1007/s00248-013-0297-x
27. Ceri, H., et al., *The Calgary Biofilm Device: new technology for rapid determination of antibiotic susceptibilities of bacterial biofilms.* J Clin Microbiol, 1999. **37**(6): p. 1771-6.
28. Hoffman, L.R., et al., *Aminoglycoside antibiotics induce bacterial biofilm formation.* Nature, 2005. **436**(7054): p. 1171-5. 10.1038/nature03912
29. Kiran, S., et al., *Enzymatic quorum quenching increases antibiotic susceptibility of multidrug resistant Pseudomonas aeruginosa.* Iran J Microbiol, 2011. **3**(1): p. 1-12.
30. Kaplan, J.B., *Antibiotic-induced biofilm formation.* Int J Artif Organs, 2011. **34**(9): p. 737-51. 10.5301/ijao.5000027
31. Sailer, F.C., B.M. Meberg, and K.D. Young, *beta-Lactam induction of colanic acid gene expression in Escherichia coli.* FEMS Microbiol Lett, 2003. **226**(2): p. 245-9.
32. Atkinson, S. and P. Williams, *Quorum sensing and social networking in the microbial world.* J R Soc Interface, 2009. **6**(40): p. 959-78. 10.1098/rsif.2009.0203
33. de Kievit, T.R. and B.H. Iglewski, *Bacterial quorum sensing in pathogenic relationships.* Infect Immun, 2000. **68**(9): p. 4839-49.
34. Ng, W.L. and B.L. Bassler, *Bacterial quorum-sensing network architectures.* Annu Rev Genet, 2009. **43**: p. 197-222. 10.1146/annurev-genet-102108-134304

35. Sakuragi, Y. and R. Kolter, *Quorum-sensing regulation of the biofilm matrix genes (pel) of Pseudomonas aeruginosa.* J Bacteriol, 2007. **189**(14): p. 5383-6. 10.1128/JB.00137-07
36. Quinones, B., G. Dulla, and S.E. Lindow, *Quorum sensing regulates exopolysaccharide production, motility, and virulence in Pseudomonas syringae.* Mol Plant Microbe Interact, 2005. **18**(7): p. 682-93. 10.1094/MPMI-18-0682
37. von Bodman, S.B., D.R. Majerczak, and D.L. Coplin, *A negative regulator mediates quorum-sensing control of exopolysaccharide production in Pantoea stewartii subsp. stewartii.* Proc Natl Acad Sci U S A, 1998. **95**(13): p. 7687-92.
38. Davies, D.G., et al., *The involvement of cell-to-cell signals in the development of a bacterial biofilm.* Science, 1998. **280**(5361): p. 295-8.
39. Tseng, B.S., et al., *The extracellular matrix protects Pseudomonas aeruginosa biofilms by limiting the penetration of tobramycin.* Environ Microbiol, 2013. **15**(10): p. 2865-78. 10.1111/1462-2920.12155
40. Shih, P.C. and C.T. Huang, *Effects of quorum-sensing deficiency on Pseudomonas aeruginosa biofilm formation and antibiotic resistance.* J Antimicrob Chemother, 2002. **49**(2): p. 309-14.
41. Davenport, E.K., D.R. Call, and H. Beyenal, *Differential protection from tobramycin by extracellular polymeric substances from Acinetobacter baumannii and Staphylococcus aureus biofilms.* Antimicrob Agents Chemother, 2014. **58**(8): p. 4755-61. 10.1128/AAC.03071-14
42. Brackman, G., et al., *The Quorum Sensing Inhibitor Hamamelitannin Increases Antibiotic Susceptibility of Staphylococcus aureus Biofilms by Affecting Peptidoglycan Biosynthesis and eDNA Release.* Sci Rep, 2016. **6**: p. 20321. 10.1038/srep20321
43. Machineni, L., et al., *Influence of Nutrient Availability and Quorum Sensing on the Formation of Metabolically Inactive Microcolonies Within Structurally Heterogeneous Bacterial Biofilms: An Individual-Based 3D Cellular Automata Model.* Bull Math Biol, 2017. **79**(3): p. 594-618. 10.1007/s11538-017-0246-9
44. Fagerlind, M.G., et al., *Dynamic modelling of cell death during biofilm development.* J Theor Biol, 2012. **295**: p. 23-36. 10.1016/j.jtbi.2011.10.007
45. Picioreanu, C., J.U. Kreft, and M.C. Van Loosdrecht, *Particle-based multidimensional multispecies biofilm model.* Appl Environ Microbiol, 2004. **70**(5): p. 3024-40.
46. Eberl H, M.E., Noguera D, Picioreanu C, Rittmann B, van Loosdrecht M, Wanner O *Mathematical modeling of biofilms.* IWA Publishing, 2006.
47. Castro, S.L., et al., *Induction of attachment-independent biofilm formation and repression of Hfq expression by low-fluid-shear culture of Staphylococcus aureus.* Appl Environ Microbiol, 2011. **77**(18): p. 6368-78. 10.1128/AEM.00175-11
48. Guo, P., A.M. Weinstein, and S. Weinbaum, *A hydrodynamic mechanosensory hypothesis for brush border microvilli.* Am J Physiol Renal Physiol, 2000. **279**(4): p. F698-712.
49. Picioreanu, C., M.C. Van Loosdrecht, and J.J. Heijnen, *Effect of diffusive and convective substrate transport on biofilm structure formation: a two-dimensional modeling study.* Biotechnol Bioeng, 2000. **69**(5): p. 504-15.
50. Falsetta, M.L., et al., *Symbiotic relationship between Streptococcus mutans and Candida albicans synergizes virulence of plaque biofilms in vivo.* Infect Immun, 2014. **82**(5): p. 1968-81. 10.1128/IAI.00087-14
51. Pizarro, G.E., et al., *Two-dimensional cellular automaton model for mixed-culture biofilm.* Water Sci Technol, 2004. **49**(11-12): p. 193-8.
52. Fozard, J.A., et al., *Inhibition of quorum sensing in a computational biofilm simulation.* Biosystems, 2012. **109**(2): p. 105-14. 10.1016/j.biosystems.2012.02.002
53. Frederick, M.R., et al., *A mathematical model of quorum sensing regulated EPS production in biofilm communities.* Theor Biol Med Model, 2011. **8**: p. 8. 10.1186/1742-4682-8-8

54. Chambless, J.D., S.M. Hunt, and P.S. Stewart, *A three-dimensional computer model of four hypothetical mechanisms protecting biofilms from antimicrobials.* Appl Environ Microbiol, 2006. **72**(3): p. 2005-13. 10.1128/AEM.72.3.2005-2013.2006
55. Schaule, G., H.C. Flemming, and H.F. Ridgway, *Use of 5-cyano-2,3-ditolyl tetrazolium chloride for quantifying planktonic and sessile respiring bacteria in drinking water.* Appl Environ Microbiol, 1993. **59**(11): p. 3850-7.
56. Manuel, C.M., O.C. Nunes, and L.F. Melo, *Dynamics of drinking water biofilm in flow/non-flow conditions.* Water Res, 2007. **41**(3): p. 551-62. 10.1016/j.watres.2006.11.007
57. Leisner, M., et al., *Kinetics of genetic switching into the state of bacterial competence.* Biophys J, 2009. **96**(3): p. 1178-88. 10.1016/j.bpj.2008.10.034
58. Ardre, M., et al., *An individual-based model for biofilm formation at liquid surfaces.* Phys Biol, 2015. **12**(6): p. 066015. 10.1088/1478-3975/12/6/066015
59. Cerca, N., et al., *Effects of growth in the presence of subinhibitory concentrations of dicloxacillin on Staphylococcus epidermidis and Staphylococcus haemolyticus biofilms.* Appl Environ Microbiol, 2005. **71**(12): p. 8677-82. 10.1128/AEM.71.12.8677-8682.2005
60. Hunt, S.M., et al., *Hypothesis for the role of nutrient starvation in biofilm detachment.* Appl Environ Microbiol, 2004. **70**(12): p. 7418-25. 10.1128/AEM.70.12.7418-7425.2004
61. Shen, Y., et al., *Experimental and Theoretical Investigation of Multispecies Oral Biofilm Resistance to Chlorhexidine Treatment.* Sci Rep, 2016. **6**: p. 27537. 10.1038/srep27537
62. Roldan, M.H.-M.a.M., *Characterization of Photosynthetic Biofilms from Roman Catacombs via 3D Imaging and Subcellular Identification of Pigments.* COALITION, 2007(15).
63. Koerber, A.J., et al., *A mathematical model of partial-thickness burn-wound infection by Pseudomonas aeruginosa: quorum sensing and the build-up to invasion.* Bull Math Biol, 2002. **64**(2): p. 239-59. 10.1006/bulm.2001.0272
64. Moskowitz, S.M., et al., *Clinically feasible biofilm susceptibility assay for isolates of Pseudomonas aeruginosa from patients with cystic fibrosis.* J Clin Microbiol, 2004. **42**(5): p. 1915-22.

822 Table I. Model parameters

Parameter	Description	Value	Unit	Reference
Δx	Element length	3	μm	
	Thickness of the DBL	18	μm	[43]
N	Number of elements in the x direction	40		
N_0	Initial number of bacterial cells	6		
m	Maintenance coefficient	0.036	h^{-1}	[43]
μ^{max}	Maximum specific growth rate of bacterial population	0.3125	h^{-1}	[43]
Y_{NB}	Yield coefficient for biomass	0.45		[43]
t^{SP}	Time in the stationary phase at which cell death occurs	24	h	[43]
R^{min}	Ratio of the rate of nutrient consumption to that of endogenous metabolism below which cell death occurs	0.15		[43]
	Threshold biomass at which cell division occurs	2×10^{-12}	g	
D_N	Diffusion coefficient of nutrient	0.84×10^{-6}	$m^2 h^{-1}$	[43]
K_N	Monod saturation constant	2.55	$g m^{-3}$	[43]
$C_{N,bulk}$	Bulk nutrient concentration	4	$g m^{-3}$	
Y_{EN}	Yield coefficient for EPS	0.27		[43]
	Threshold concentration at which EPS division occurs	33000	$g m^{-3}$	[43]
D_A	Diffusion coefficient of autoinducer	1×10^{-6}	$m^2 h^{-1}$	
P_{Au}	Autoinducer production rate by up-regulated cells	73800	$molecules\ h^{-1}$ [52]	[52]
P_{Ad}	Autoinducer production rate by down-regulated cells	498	$molecules\ h^{-1}$ [52]	[52]
α	Spontaneous up-regulation rate	7.89×10^{-17}	$molecules\ h^{-1}$ [52] $m^3 molecule^{-1} h^{-1}$ [52, 63]	[52, 63]
β	Spontaneous down-regulation rate	0.975	h^{-1}	[52, 63]

γ	Transition constant	7.96×10^{-17}	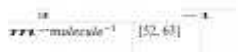	[52, 63]
D^{ab}	Diffusion coefficient of antibiotic	0.36×10^{-6}	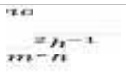	[54]
$\frac{D^{ab}}{K^{ab}}$	Antibiotic half-saturation coefficient	1	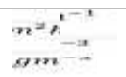	[54]
K^{abMax}	Maximum specific reaction rate of antibiotic with bacterial cell	2.5	h^{-1}	[54]
BIC	Biofilm inhibitory concentration	1- 64	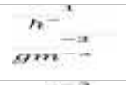	[64]
K^{EPSMax}	Maximum specific reaction rate of antibiotic with EPS	0.25	h^{-1}	

823